International Journal of Automation and Computing 17(3), June 2020, 403-416
DOI: 10.1007/s11633-020-1228-1

Design and Analysis of a Novel Hybrid Processing Robot Mechanism

Hai-Rong Fang Tong Zhu Hai-Qiang Zhang Hui Yang Bing-Shan Jiang

School of Mechanical, Electronic and Control Engineering, Beijing Jiaotong University, Beijing 100044, China

Abstract: In order to satisfy the requirements of large workspace and high dexterity for processing equipment of oversized cylindrical boxes′ spherical crown surfaces in the aerospace industry, a novel serial-parallel hybrid processing robot mechanism is proposed. The degrees of freedom of the 5PUS-(2UR)PU parallel mechanism are obtained by using the screw theory. The inverse kinematics of the hybrid mechanism are analyzed and the velocity Jacobian matrix is established. Then, the constraints of the main factors influencing workspace of the mechanism are given, and the position and posture workspace are obtained. Next, the dexterity and stiffness performance of the mechanism is analyzed based on the Jacobian matrix. The virtual prototype is established, and the theoretical calculation and simulation analysis of the hybrid mechanism with arc curve as the processing trajectory are carried out by using Matlab and Adams software. The research results show that the mechanism can satisfy the requirements of large workspace and high dexterity of oversized cylindrical boxes′ spherical crown surface processing, and has feasibility and practical application value.

Keywords: Hybrid mechanism, kinematic analysis, large workspace, dexterity, kinematic simulation.

1 Introduction

At present, there are technical difficulties in the processing of spherical crown surfaces on oversized cylindrical boxes in the aerospace field. First of all, due to the huge size of the box structure, the processing equipment is required to have a large processing space. Secondly, the box is a thin-walled structure with severe deformation, and the traditional forming and processing methods cannot satisfy the processing requirements. Finally, the surface of the box has a complicated structure, which requires that processing equipment has higher dexterity. However, existing computerized numerical control (CNC) machine tools, serial robots, and parallel robots cannot satisfy their processing requirements. Therefore, it is necessary to design a robot mechanism that satisfies the requirements for processing of oversized cylindrical boxes′ spherical crown surface.

Due to the large size, serious deformation and complicated convex structure of the cylindrical box, the processing robot is required to have a large workspace. The focus is on the large displacement along the axis of the box. At the same time, the processing robot is required to have high dexterity. Serial robots have been widely used in industrial production because of their advantages of flexible operation and large workspace, such as PUMA (programmable universal machine for assembly)[1], SCARA (selective compliance assembly robot arm)[2] and IRB (industrial robots)[3]. However, the serial robots also have the disadvantage of small stiffness. Parallel robots have many obvious advantages compared with traditional serial robots, such as high accuracy, high stiffness, and small error accumulation[4-7], which are applied to parallel machining machines[8,9]. But parallel robots also have the disadvantage of small workspace.

A hybrid robot is a combination of serial and parallel robots, or a sequence of two parallel robots[10]. The hybrid robots overcome the limited workspace of the parallel robots and combine the advantages of large workspace, high dexterity and high stiffness of serial robots and parallel robots[11-13], which can satisfy the requirements for processing of oversized boxes to the greatest extent.

Hybrid robots have been widely used in aerospace and automotive processing, such as Tricept robot[14] and Exechon robot[15, 16]. At present, the design of the hybrid robot mechanism can be divided into two categories[17]. The first is a two-degree-of-freedom (2-DOF) rotating head in series at the end of a parallel mechanism. For example, Huang et al.[18, 19] proposed a Trivariant hybrid robot based on the Tricept robot, which has a large workspace. Dong et al.[20], Song et al.[21] proposed a novel 5-DOF hybrid mechanism by connecting a 2-DOF rotating head at the end of a 3-DOF parallel mechanism. And the kinematics and stiffness modeling are analyzed. The second type is a combination of guide rails or rotary platforms and parallel mechanisms. For example, Yang et al.[22, 23]

Research Article
Manuscript received December 25, 2019; accepted February 12, 2020; published online April 2, 2020
Recommended by Associate Editor Xun Xu

proposed a large-workspace hybrid robot mechanism by connecting circular guides to a fixed platform. Designing new manipulator structures is defined as type synthesis that has been the interest of many authors recently. They are considered type synthesis as a geometrical constraint problem and defined distance and angular constraints between points, lines, and planes on the base and moving platforms[24]. Xie et al.[25] proposed several 3-DOF parallel mechanisms through the type synthesis, and combined them with 1T1R (T denotes translation and R denotes rotation) worktable to obtain the hybrid machine tools. Kakinuma et al.[26] developed a 5-DOF portable hybrid polishing machine by connecting a fixed platform with a two-way moving guide rail.

The control of a hybrid robot is very complicated. Regular shape trajectories are important in application environment of the industrial robots since robots are easily controlled in regular-shaped workspaces[10]. In order to reduce the complexity of control during processing, the entire box spherical crown surface is divided into many small cylindrical areas with the same shape. The parallel processing head of the hybrid robot completes the processing of a local cylindrical area and moves to the next cylindrical area to complete the processing. At the same time, the trimming process of locally complex protrusions is completed. By analogy, the processing of the spherical crown of the entire box is completed.

In this paper, a hybrid robot mechanism for spherical processing of oversized boxes is designed. The workspace of the robot can cover the entire spherical crown surface. The remainder of this article is given as follows. In Section 2, the hybrid mechanism is designed according to the processing requirements, and the degrees of freedom are obtained for the parallel mechanism. The analysis of kinematics including inverse solution and velocity Jacobian matrix is conducted in Section 3. Section 4 analyzes the performance of the hybrid mechanism. In Section 5, the kinematic simulation of the mechanism is analyzed and compared with the theoretical calculation. Finally, conclusions are given in Section 6.

2 Configuration design and freedom calculation

2.1 Configuration design

The structural design of the mechanism requires the mechanism to have a large stroke in the vertical direction. And a single parallel mechanism, because of the small workspace, is difficult to satisfy the needs of large stroke in the vertical direction. Therefore, it is necessary to connect a large-stroke mechanism in series on the basis of a parallel mechanism to achieve the design requirements by a hybrid connection.

For the structure configuration of the large stroke part, the expandable mechanism can be a good choice to satisfy the large stroke and reduce the size of the processing equipment as much as possible. The expandable mechanism is composed of connecting links, connectors and rollers, which is shown in Fig. 1 (a). The connecting links are connected with the connectors and rollers, and the mechanism can expand and contract in the vertical direction. In order to increase the stiffness of the mechanism, a pentahedral structure based on the expandable mechanism is adopted, and a lifting adjustment device (LAD) is obtained, as shown in Fig. 1 (b). The five expandable mechanisms are arranged in a space pentahedron. The structure can withstand forces in different directions, which has higher stiffness and a larger stroke-to-size ratio.

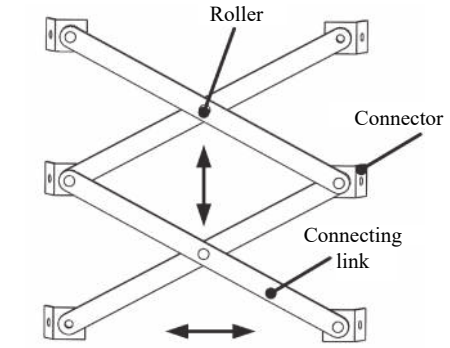

(a) Expandable mechanism

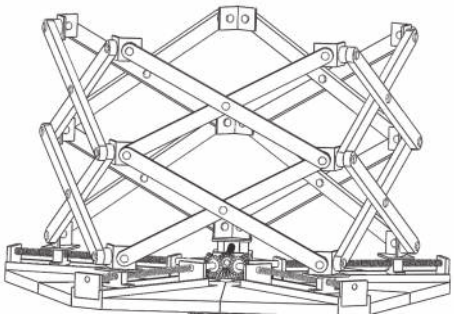

(b) Structure of LAD

Fig. 1 Structural configuration of large stroke

For the configuration of the parallel part, because the spherical surface of the box is a complex curved surface, the mechanism is required to have at least 5 degrees of freedom (3T2R). Therefore, five 6-DOF branches are used as actuated branches, and a 5-DOF constrained branch is added as a passive branch, which is the basic configuration of the parallel mechanism.

For the design of the actuated branch, in order to increase the vertical stroke, a PRR (P denotes the prismatic joint, R denotes the revolute joint) passive branch is connected on the basis of the PUS (U denotes the universal joint, S denotes the spherical joint) actuated branch, as shown in Fig. 2. The prismatic joint in the PRR passive branch is fixedly connected with the connector of the

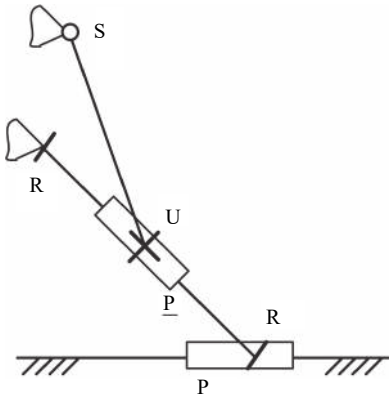

Fig. 2 Schematic diagram of parallel branch

LAD, which can move along the guide rail with the connector. This article classifies the PRR passive branch into the LAD. The P joint of the PUS branch is the actuated joint. This structure configuration can achieve the secondary superposition of vertical displacement.

The structure of the constrained branch is shown in Fig. 3. And two U joints and R joints are connected to form a 2UR closed-loop structure. There are U and P joints at the top. The structure uses R joints instead of P joints, which makes the structure compact, effectively increases the strength of the branch, and avoids self-locking due to excessive P joints.

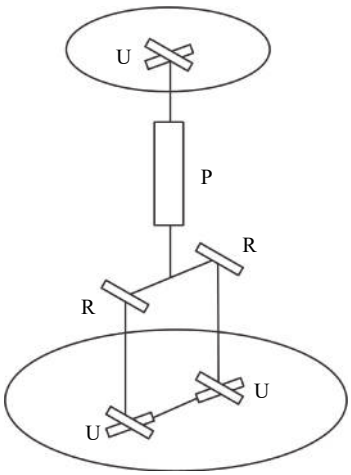

Fig. 3 Schematic diagram of constrained branch

The schematic diagram of the overall processing system is shown in Fig. 4 (a). It is mainly composed of a hybrid mechanism, a horizontal rail, longitudinal rails, and brackets. The hybrid mechanism can be moved along the horizontal and longitudinal guide rails. With the degrees of freedom of the hybrid mechanism, the end processing head can reach the entire spherical crown surface of the box.

The machining system uses a machining scheme for local real-time milling of the parallel mechanism. That is, when the parallel mechanism moves to a position on the

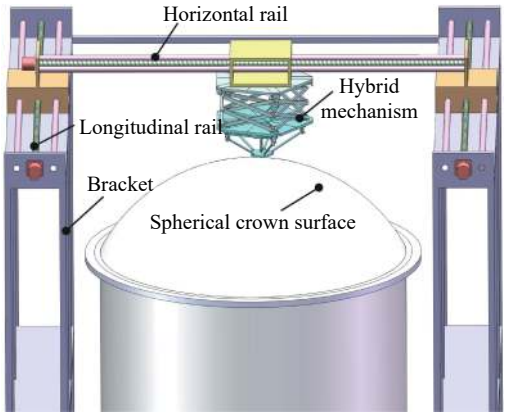

(a) Overall processing system

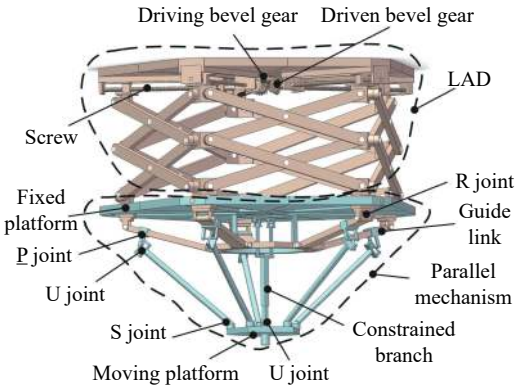

(b) A 3D model of hybrid mechanism

Fig. 4 Serial-parallel processing robot system

surface of the box, it is automatically scanned and detected. Based on the 5 degrees of freedom of the parallel mechanism, the milling of local profiles is completed. Then, it moves to the next position to complete the milling of another profile, etc. The processing of the spherical crown surface is completed. This processing system solution can eliminate the accumulated errors of large long guide rails and LADs. It has lower requirements for the accuracy of the guide rails and LADs, and relatively reduces the cost. Through the positioning of the local parallel mechanism, the local profile processing can be completed, which can achieve higher processing accuracy. During the entire processing process, the end-effector of the hybrid robot mainly fulfills two tasks. The first is to complete the washing process of the fixed cylindrical area. The second step is to complete the 5-DOF trimming process for locally complex protruding structures.

This paper mainly analyzes the part of the hybrid mechanism. The 3D model of the new hybrid mechanism is shown in Fig. 4 (b). The mechanism consists of a LAD, a fixed platform, a moving platform, 5 identical PUS active branches and a (2UR)PU passive branch. Active and passive branch chains connect fixed platforms and moving platforms. The LAD is mainly composed of a central driving bevel gear, five driven bevel gears, lead screws, a

shear fork group and five identical PRR passive lifting branch chains. When the active bevel gear rotates, it drives the shear bar group and the PRR passive branch chain to contract inward. At the same time, the whole parallel mechanism part is moved vertically. The active branches of the parallel mechanism are evenly connected to the fixed platform. Each active branch is composed of a P joint, a U joint, and a S joint. P is the actuated joint and is driven by a linear motor. For the passive branch chain, it consists of a 2UR closed-loop structure, a P joint and a U joint, where the U joint is connected to the moving platform.

The structure of the parallel mechanism is shown in Fig. 5. A_i is the center of the S joint connected to the moving platform on the i-th (i=1, 2, ⋯, 5) active branch chain of the mechanism, and the center of the U joint connected to the actuated P joint is C_i. B is the center of the fixed platform. A is the center of the moving platform. And D is the center of the middle platform. The fixed platform $B_1B_2B_3B_4B_5$ is a regular pentagon, and the moving platform $A_1A_2A_3A_4A_5$ is a symmetrical pentagon. The joint points A_i (i=2, 3, ⋯, 5) are evenly distributed, and the interval angle is 90°. A fixed coordinate system B-$x_0y_0z_0$ and a moving coordinate system A-uvw as shown in Fig. 5 are established. The direction of the x_0 axis is from B to B_1. The z_0-axis direction is vertically upward. The u-axis direction is from A to A_1. And the w-axis direction is vertically upward.

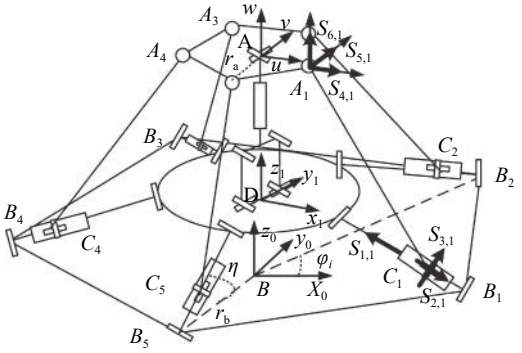

Fig. 5 Schematic diagram of the parallel mechanism

2.2 Degrees of freedom

The movement of the hybrid mechanism is divided into two parts. When the actuated P joint of the parallel part is locked, it is driven by the LAD, and the whole mechanism will move in the z-axis direction. When the LAD is locked, the degree of freedom of the hybrid mechanism is determined by the 5PUS-(2UR)PU parallel mechanism part. Because five identical PUS active branches are unconstrained branches, the degree of freedom of the 5PUS-(2UR)PU mechanism is determined by the (2UR)PU constrained branch.

The screw theory is used to analyze the constrained branches[27]. The schematic diagram of the kinematic screw system and coordinate system of the intermediate constrained branch chain is shown in Fig. 6. The directions of the x_D axis and the y_D axis are respectively along the two rotation axes of the U joint. Assume the position of each point in the branch chain relative to the coordinate system D_1-$x_Dy_Dz_D$ is: $D_2(0,\ y_{D2},\ z_{D2})$ $D_3(0,\ y_{D3},\ 0)$ $D_4(0,\ y_{D2}+y_{D3},\ z_{D2})$ $D_5(0,\ y_{D5},\ z_{D5})$. The direction vector of the z_7 axis is $(m_{D5},\ 0,\ n_{D5})$.

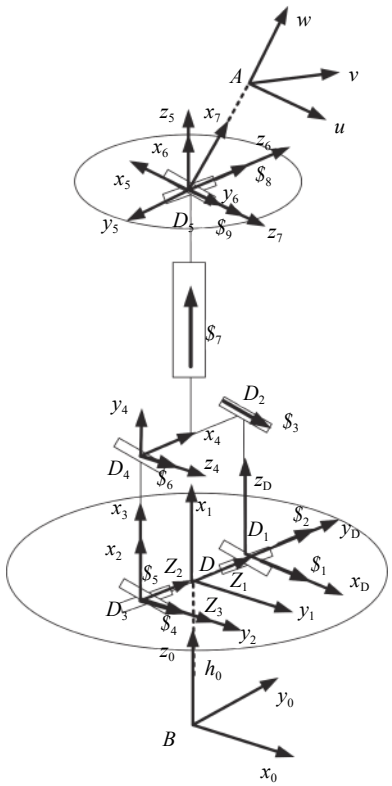

Fig. 6 Kinematic screw and coordinate system of (2UR)PU branch

As for the (2UR)PU branch chain, it contains the 2UR closed-loop chain, which can be regarded as a general kinematic pair. The kinematic screw of the D_1D_2 branch in the 2UR closed-loop chain can be easily obtained as

$$\begin{cases} \$_1 = [100; 000] \\ \$_2 = [010; 000] \\ \$_3 = [100; 0z_{D2}\ -y_{D2}]. \end{cases} \tag{1}$$

The reciprocal screw of (1) is obtained as

$$\begin{cases} \$^r_{11} = [1\ 0\ 0; 0\ 0\ 0] \\ \$^r_{12} = [0\ y_{D2}\ z_{D2}; 0\ 0\ 0] \\ \$^r_{13} = [0\ 0\ 0; 0\ 0\ 1]. \end{cases} \tag{2}$$

where $\$^r_{11}$ and $\$^r_{12}$ represent two constraint forces along the x-axis and D_1D_2 directions, respectively. $\$^r_{13}$

represents a constraint force couple, along the z-axis direction.

Because the left and right branches are the same and the reciprocal screw is also the same, the maximum unrelated reciprocal screw group for the D_2D_4 link is obtained as

$$\begin{cases} \$_1^{\mathrm{r}} = [1\ 0\ 0; 0\ 0\ 0] \\ \$_2^{\mathrm{r}} = [0\ y_{\mathrm{D2}}\ z_{\mathrm{D2}}; 0\ 0\ 0] \\ \$_3^{\mathrm{r}} = [0\ 0\ 0; 0\ 0\ 1] \\ \$_4^{\mathrm{r}} = [0\ y_{\mathrm{D2}}\ z_{\mathrm{D2}}; y_{D3}z_{D2}\ 0\ 0]. \end{cases} \tag{3}$$

Based on the reciprocal screw system of (3), the basic kinematic screw of D_2D_4 link can be obtained as

$$\begin{cases} \$_{11} = [0\ 1\ 0; 0\ 0\ 0] \\ \$_{22} = [0\ 0\ 0; 0\ z_{\mathrm{D2}}\ -y_{\mathrm{D2}}]. \end{cases} \tag{4}$$

Then, the kinematic screw system of (2UR)PU branch can be expressed as

$$\begin{cases} \$_{11} = [0\ 1\ 0; 0\ 0\ 0] \\ \$_{22} = [0\ 0\ 0; 0\ z_{\mathrm{D2}}\ -y_{\mathrm{D2}}] \\ \$_7 = [0\ 0\ 0; 0\ 0\ z_{\mathrm{D5}}] \\ \$_8 = [0\ 1\ 0; -z_{\mathrm{D5}}\ 0\ 0] \\ \$_9 = [m_{\mathrm{D5}}\ 0\ n_{\mathrm{D5}}; y_{\mathrm{D5}}n_{\mathrm{D5}}\ z_{\mathrm{D5}}m_{\mathrm{D5}}\ -m_{\mathrm{D5}}y_{\mathrm{D5}}]. \end{cases} \tag{5}$$

Based on the kinematic screw system of (5), we can get the constraint screw of the (2UR)PU branch as:

$$\$^{\mathrm{r}} = [0\ 0\ 0; -n_{\mathrm{D5}}\ 0\ m_{\mathrm{D5}}]. \tag{6}$$

Equation (6) represents a constraint force couple whose direction is around the plane normal direction formed by the two rotation axes of the U pair connected to the moving platform. Therefore, the constraint force couple constrains the rotation of the moving platform around its normal direction. Then the 5PUS-(2UR)PU parallel mechanism is a 5-DOF mechanism (3T2R), that is, three translations along the x, y, and z axes and two rotations around the x, y axes.

3 Kinematic analysis

Establish the coordinate system as shown in Fig. 5, and assume the parameters in the mechanism as follows: AA_i=r_{a}, BB_i=r_{b}, C_iA_i=l (i=1, 2, ⋯, 5). Parameter ϕ_i is the angle measured from x_0 axis to vector $\boldsymbol{BB}_i$, ϕ_i is the angle measured from u axis to vector $\boldsymbol{AA}_i$ and η is the angle measured from u axis to vector $\boldsymbol{AA}_i$. Parameter $\boldsymbol{a}_i$ and $\boldsymbol{b}_i$ represent the position vector of joint A_i and B_i in the fixed coordinate system B-$x_0y_0z_0$, respectively. The $\boldsymbol{B}_i\boldsymbol{C}_i$ direction vector is $\boldsymbol{s}_{i0}$, and the $\boldsymbol{C}_i\boldsymbol{A}_i$ direction vector is $\boldsymbol{l}_{i0}$. $\boldsymbol{R}$ represents the rotation transformation matrix of the moving coordinate system A-uvw relative to the fixed coordinate system B-$x_0y_0z_0$.

Assume β being the angle that the moving platform rotates around the u axis, and α being the angle that the moving platform rotates around the v axis. During the coordinate transformation, the angle α is first rotated around the v axis, and then the angle β is rotated around the u axis. The rotation matrices are expressed as $\boldsymbol{R}_v(\alpha)$ and $\boldsymbol{R}_u(\beta)$, respectively. The total transformation matrix can be represented as

$$\boldsymbol{R} = \boldsymbol{R}v\,(\alpha)\ \boldsymbol{R}u\,(\beta)\,. \tag{7}$$

The position vector of B_i in the fixed coordinate system B-$x_0y_0z_0$ can be obtained as

$$\boldsymbol{b}_i = r_{\mathrm{b}}\,[\cos\varphi_i, \sin\varphi_i, 0]^{\mathrm{T}}. \tag{8}$$

The position vector of A_i in the moving coordinate system A-uvw can be obtained as

$${}^{\mathrm{A}}\boldsymbol{a}_i = r_{\mathrm{a}}\,[\cos\phi_i, \sin\phi_i, 0]^{\mathrm{T}}. \tag{9}$$

According to the rotation transformation matrix, the position vector of A_i in the fixed coordinate system B-$x_0y_0z_0$ can be expressed as

$$\boldsymbol{a}_i = \boldsymbol{R}^{\mathrm{A}}\boldsymbol{a}_i. \tag{10}$$

3.1 Inverse kinematics of parallel mechanism

For the 5PUS-(2UR)PU parallel mechanism part, assume that the pose parameter of the center A relative to the coordinate system B-$x_0y_0z_0$ is $\boldsymbol{r} = [x, y, z, \alpha, \beta]^{\mathrm{T}}$. And the direction vector of the actuated P joint can be obtained as

$$\boldsymbol{s}_{i0} = [-\cos\varphi_i\cos\eta,\ -\sin\varphi_i\cos\eta, \sin\eta]^{\mathrm{T}}. \tag{11}$$

Based on the close-loop vector method, establish the constraint equation as

$$\boldsymbol{L}_i = \boldsymbol{B}_i\boldsymbol{A}_i = -\boldsymbol{b}_i + \boldsymbol{r} + \boldsymbol{a}_i = s_i\boldsymbol{s}_{i0} + l_i\boldsymbol{l}_{i0}. \tag{12}$$

Taking the square of both sides of (12) yields

$${s_i}^2 - 2\boldsymbol{L}_i\boldsymbol{s}_{i0}s_i + {\boldsymbol{L}_i}^{\mathrm{T}}\boldsymbol{L}_i - l^2 = 0. \tag{13}$$

By solving the equation of s_i from (13), the translation of the actuated P joint can be obtained as

$$s_i = {\boldsymbol{L}_i}^{\mathrm{T}}\boldsymbol{s}_{i0} \pm \sqrt{({\boldsymbol{L}_i}^{\mathrm{T}}\boldsymbol{s}_{i0})^2 - {\boldsymbol{L}_i}^{\mathrm{T}}\boldsymbol{L}_i + l^2} \tag{14}$$

where i = 1, 2, ⋯, 5.

3.2 Positive forward of vertical translation

The movement of the hybrid mechanism is divided in-

to the overall vertical movement and the 5-DOF movement of the local 5PUS-(2UR)PU parallel mechanism. When the end moving platform moves vertically only along the z_0 axis, and the driving displacement r_b of the LAD and the displacement s_i (i=1, 2, ⋯, 5) of the actuated P joint are known, the vertical translation z of the moving platform can be solved.

Because the LAD has a regular pentagonal structure, the included angle of the drive axis is 54°. The length of the connecting link is l_b. From the structure of a right-angled triangle, the vertical translation of the LAD can be obtained as

$$z_b = 2\sqrt{{l_b}^2 - 4{r_b}^2\cos(54°)^2}. \tag{15}$$

Assume that the position vector of $\boldsymbol{BA}$ in the coordinate system B-$x_0y_0z_0$ is $\boldsymbol{r}_2 = [0, 0, z_a]^T$. And the posture angles α and β are 0. Since there is only one unknown, the constraint equation of the parallel part driving branch 1 can be established by (12):

$$-\boldsymbol{b}_1+\boldsymbol{r}_2+\boldsymbol{a}_1=s_1\boldsymbol{s}_{10}+l_1\boldsymbol{l}_{10} \tag{16}$$

Substituting (8), (10) and (10) into (16) and squaring both sides of (16) can be deduced as

$$z_a = \sqrt{l^2 - (r_a - r_b + s_1\cos\eta)^2} + s_1\sin\eta. \tag{17}$$

Adding (15) and (17) gives a total vertical translation as

$$z = z_b + z_a. \tag{18}$$

3.3 Inverse kinematics of constrained branch

The D-H method is used to analyze the inverse kinematics of (2UR)PU constrained branches. Establish coordinate systems as shown in Fig. 6, where z_2, z_3, z_6 and z_7 are along the axis of the U joint, z_4 is along the axis of the R joint, and z_5 is along the moving direction of the P joint.

The displacement of the coordinate system D-$x_1y_1z_1$ of the middle branch relative to the fixed coordinate system B-$x_0y_0z_0$ is: (0, 0, h_0). The Euler angle of Z-Y-X is (–π/2, –π/2, 0). The displacement of the coordinate system A-uvw relative to the coordinate system D_5-$x_7y_7z_7$ is (h_1, 0, 0), and the Euler angle of Z-Y-X is (π, –π/2, 0). The D-H parameters of the middle branch are shown in Table 1.
where θ_1, θ_2, θ_5, θ_6, and d_4 are variables, g_2 and g_3 are constants.

From Table 1 the transformation matrix of the moving platform coordinate system A-uvw relative to the fixed platform coordinate system B-$x_0y_0z_0$ can be obtained as

Table 1 D-H parameters of constrained branch

Link i	Torsional angle γ_{i-1} (°)	Length g_{i-1}	Offset distance d_i	Joint angle θ_i (°)
1	0	0	0	θ_1
2	−90	0	0	θ_2
3	0	g_2	0	$-\theta_2-90$
4	−90	g_3	d_4	90
5	90	0	0	θ_5
6	−90	0	0	θ_6

$$\boldsymbol{T}_{A-B}(\theta_1,\theta_1,\theta_1,\theta_1,d_4) = \begin{bmatrix} s(\theta_1+\theta_5) & -c(\theta_1+\theta_5)s\theta_6 & -c(\theta_1+\theta_5)s\theta_6 & \\ 0 & c\theta_6 & -s\theta_6 & \\ c(\theta_1+\theta_5) & s(\theta_1+\theta_5)s\theta_6 & c\theta_6 s(\theta_1+\theta_5) & \\ 0 & 0 & 0 & \end{bmatrix}$$
$$\begin{bmatrix} (g_2c\theta_2+d_4)(s\theta_1) - h_1c(\theta_1+\theta_5)c\theta_6 \\ -g_2s\theta_2 - h_1s\theta_6 \\ h_0 + c\theta_1(g_2c\theta_2+d_4+h_1s\theta_5c\theta_6) + h_1s\theta_1c\theta_5c\theta_6 \\ 1 \end{bmatrix} \tag{19}$$

where s and c are the abbreviations of sine and cosine.

The Y-X-Z Euler angle (α, β, γ) is used to represent the posture of the moving platform. The displacement is (x, y, z). Then the transformation matrix of the moving coordinate system A-uvw relative to the fixed coordinate system B-$x_0y_0z_0$ can be expressed as

$$\boldsymbol{T}_{A-B}(x,y,z,\alpha,\beta,\gamma) = \begin{bmatrix} c\alpha c\gamma + s\alpha s\beta s\gamma & c\gamma s\alpha s\beta - c\alpha s\gamma & c\beta s\alpha & x \\ c\beta s\gamma & c\beta c\gamma & -s\beta & y \\ c\alpha s\beta s\gamma - c\gamma s\alpha & c\alpha s\beta c\gamma + s\alpha s\gamma & c\alpha c\beta & z \\ 0 & 0 & 0 & 1 \end{bmatrix}. \tag{20}$$

The parameters of the matrix in (19) and (20) correspond to each other.

$$\begin{cases} x = s\theta_1(g_2c\theta_2+d_4) - h_1c(\theta_1+\theta_5)c\theta_6 \\ y = -g_2s\theta_2 - h_1s\theta_6 \\ z = h_0 + c\theta_1(g_2c\theta_2+d_4) + h_1s(\theta_1+\theta_5)c\theta_6 \\ \alpha = (\theta_1+\theta_5) - \pi/2 \\ \beta = \theta_6 \\ \gamma = 0°. \end{cases} \tag{21}$$

It can be seen from (21) that $\gamma = 0°$. Therefore, the rotation parameter of the moving platform around the z axis (the moving platform coordinate normal) is 0°, which is a constant. The rotational angular velocity of the moving platform around its normal is 0. It can be known that in the movement of the mechanism, the 2UR-PU middle

constraint branch will always constrain the rotation of the moving platform around its normal direction. This is consistent with the conclusions analyzed by the screw theory.

When the posture parameters (x, y, z, α, β) of the moving platform are known, the joint parameters (θ_1, θ_2, θ_5, θ_6, d_4) of the middle constraint branch can be determined as

$$\begin{cases} \theta_2 = \arcsin\left(-\dfrac{y + h_1 s\beta}{g_2}\right) \\ d_4 = -g_2 c\theta_2 + \\ \sqrt{(x - h_1 s\alpha c\theta_6)^2 + (z - h_0 - h_1 c\alpha c\theta_6)^2} \\ \theta_1 = \arctan\left(\dfrac{x - h_1 s\alpha c\theta_6}{z - h_0 - h_1 c\alpha c\theta_6}\right) \\ \theta_5 = \alpha - \theta_1 + \pi/2 \\ \theta_6 = \beta. \end{cases} \tag{22}$$

3.4 Jacobian matrix

The method of screw theory is used to establish the Jacobian matrix. The kinematic screw of each joint is shown in Fig. 5. $\boldsymbol{s}_{j,i}$ represents the axis direction of the j-th joint of the i-th branch. Assume the linear velocity of the actuated P joint is $\dot{q}_i$,$\dot{\boldsymbol{q}} = (\dot{q}_1 \quad \dot{q}_2 \quad \dot{q}_3 \quad \dot{q}_4 \quad \dot{q}_5)^{\mathrm{T}}$, and the output speed vector of the moving platform is $\dot{\boldsymbol{x}} = (\dot{\alpha} \quad \dot{\beta} \quad \dot{x} \quad \dot{y} \quad \dot{z})^{\mathrm{T}}$. Then, the mapping relationship between them can be expressed as

$$\boldsymbol{J}_{\mathrm{x}}\dot{\boldsymbol{x}} = \boldsymbol{J}_{\mathrm{p}}\dot{\boldsymbol{q}} \tag{23}$$

where $\boldsymbol{J}_{\mathrm{x}}$ and $\boldsymbol{J}_{\mathrm{p}}$ are called indirect and direct Jacobian matrices of the parallel mechanism, respectively.

According to the screw theory, the instantaneous velocity $\$_{\mathrm{p}} = [\ \omega^{\mathrm{T}} \quad v^{\mathrm{T}}\ ]^{\mathrm{T}}$(where v is the linear velocity of the moving platform center and ω is the angular velocity of the moving platform) of the moving platform relative to the base can be written as a linear combination of the speed and screw of each joint in each branch. And so

$$\begin{aligned} \$_{\mathrm{p}} = [\omega^{\mathrm{T}} \quad v^{\mathrm{T}}]^{\mathrm{T}} = q_i\$_{1,i} + \theta_{2,i}\$_{2,i} + \\ \theta_{3,i}\$_{3,i} + \theta_{4,i}\$_{4,i} + \theta_{5,i}\$_{5,i} + \theta_{6,i}\$_{6,i} \end{aligned} \tag{24}$$

where $i = 1, 2, \cdots, 5$, $\theta_{j,i}$ represents the angular velocity of the j-th ($j = 2, 3, \cdots, 6$) R joint in the i-th branch chain.

The kinematic screw of the joints in each branch is as follows:

$$\begin{cases} \$_{1,i} = [0;\ \boldsymbol{s}_{i0}] \\ \$_{j,i} = [\boldsymbol{s}_{j,i};\ (\boldsymbol{a}_i + \boldsymbol{l}_i) \times \boldsymbol{s}_{j,i}], \quad j = 2, 3 \\ \$_{j,i} = [\boldsymbol{s}_{j,i};\ \boldsymbol{a}_i \times \boldsymbol{s}_{j,i}], \quad j = 4, 5, 6 \end{cases} \tag{25}$$

where $\boldsymbol{l}_i = l_i\boldsymbol{l}_{i0}$.

If the actuated P joint is locked, a reciprocal screw of the branch chain can be obtained as

$$\$_i^{\mathrm{r}} = [\ \boldsymbol{l}_{i0} \quad \boldsymbol{a}_i \times \boldsymbol{l}_{i0}\ ]^{\mathrm{T}} \tag{26}$$

where $\$_i^{\mathrm{r}}$ is the unit screw passing through the center of the S joint and parallel to $\boldsymbol{l}_{i0}$.

From (24) and (26),

$$\$_i^{\mathrm{r}} \circ \$_{\mathrm{p}} = \dot{q}_i\$_i^{\mathrm{r}} \circ \$_{1,i}. \tag{27}$$

Substituting (25) and (26) into (27) and stacking 5 branches can be obtained as

$$J_{\mathrm{A}}\$_{\mathrm{p}} = \boldsymbol{J}_{\mathrm{t}}\dot{q} \tag{28}$$

where

$$\boldsymbol{J}_{\mathrm{t}} = \begin{bmatrix} \boldsymbol{l}_{10}^{\mathrm{T}}\boldsymbol{s}_{10} & 0 & 0 & 0 & 0 \\ 0 & \boldsymbol{l}_{20}^{\mathrm{T}}\boldsymbol{s}_{20} & 0 & 0 & 0 \\ 0 & 0 & \boldsymbol{l}_{30}^{\mathrm{T}}\boldsymbol{s}_{30} & 0 & 0 \\ 0 & 0 & 0 & \boldsymbol{l}_{40}^{\mathrm{T}}\boldsymbol{s}_{40} & 0 \\ 0 & 0 & 0 & 0 & \boldsymbol{l}_{50}^{\mathrm{T}}\boldsymbol{s}_{50} \end{bmatrix} \tag{29}$$

$$\boldsymbol{J}_{\mathrm{A}} = \begin{bmatrix} (\boldsymbol{a}_1 \times \boldsymbol{l}_{10})^{\mathrm{T}} & \boldsymbol{l}_{10}^{\mathrm{T}} \\ (\boldsymbol{a}_2 \times \boldsymbol{l}_{20})^{\mathrm{T}} & \boldsymbol{l}_{20}^{\mathrm{T}} \\ (\boldsymbol{a}_3 \times \boldsymbol{l}_{30})^{\mathrm{T}} & \boldsymbol{l}_{30}^{\mathrm{T}} \\ (\boldsymbol{a}_4 \times \boldsymbol{l}_{40})^{\mathrm{T}} & \boldsymbol{l}_{40}^{\mathrm{T}} \\ (\boldsymbol{a}_5 \times \boldsymbol{l}_{50})^{\mathrm{T}} & \boldsymbol{l}_{50}^{\mathrm{T}} \end{bmatrix}. \tag{30}$$

The angular velocity $\boldsymbol{\omega} = [\ \omega_{\mathrm{x}} \quad \omega_{\mathrm{y}} \quad \omega_{\mathrm{z}}\ ]^{\mathrm{T}}$ of the moving platform can also be expressed by the derivative $\boldsymbol{\omega}_1 = [\ \dot{\alpha} \quad \dot{\beta} \quad \dot{\gamma}\ ]^{\mathrm{T}}$ of the Y-X-Z Euler angle (α, β, γ) with respect to time:

$$\begin{aligned} \boldsymbol{\omega} = \boldsymbol{R}(Y,\alpha)\begin{bmatrix} 0 \\ 1 \\ 0 \end{bmatrix}\dot{\alpha} + \boldsymbol{R}(Y,\alpha)\boldsymbol{R}(X,\beta)\begin{bmatrix} 1 \\ 0 \\ 0 \end{bmatrix}\dot{\beta} + \\ \boldsymbol{R}(Y,\alpha)\boldsymbol{R}(X,\beta)\boldsymbol{R}(Z,\gamma)\begin{bmatrix} 0 \\ 0 \\ 1 \end{bmatrix}\dot{\gamma} \end{aligned} \tag{31}$$

So, simplification can be obtained as

$$\boldsymbol{\omega} = \begin{bmatrix} 0 & \cos\alpha & \cos\beta\sin\alpha \\ 1 & 0 & -\sin\beta \\ 0 & -\sin\alpha & \cos\beta\cos\alpha \end{bmatrix}\begin{bmatrix} \dot{\alpha} \\ \dot{\beta} \\ \dot{\gamma} \end{bmatrix}. \tag{32}$$

Because of $\gamma = 0$, so $\dot{\gamma} = 0$, and then

$$\begin{bmatrix} \omega_x \\ \omega_y \\ \omega_z \end{bmatrix} = \begin{bmatrix} 0 & \cos\alpha \\ 1 & 0 \\ 0 & -\sin\alpha \end{bmatrix}\begin{bmatrix} \dot{\alpha} \\ \dot{\beta} \end{bmatrix}. \tag{33}$$

Therefore, the six-dimensional velocity of the moving platform can be expressed as

$$\begin{bmatrix} \boldsymbol{\omega} \\ \boldsymbol{v} \end{bmatrix} = \boldsymbol{T}_{\mathrm{a}} \begin{bmatrix} \dot{\alpha} \\ \dot{\beta} \\ v \end{bmatrix} \tag{34}$$

where

$$\boldsymbol{T}_{\mathrm{a}} = \begin{bmatrix} 0 & \cos\alpha & 0 & 0 & 0 \\ 1 & 0 & 0 & 0 & 0 \\ 0 & -\sin\alpha & 0 & 0 & 0 \\ 0 & 0 & 1 & 0 & 0 \\ 0 & 0 & 0 & 1 & 0 \\ 0 & 0 & 0 & 0 & 1 \end{bmatrix}. \tag{35}$$

So it can be obtained as

$$\boldsymbol{J}_{\mathrm{A}}\boldsymbol{T}_{\mathrm{a}} \begin{bmatrix} \dot{\alpha} \\ \dot{\beta} \\ v \end{bmatrix} = \boldsymbol{J}_{\mathrm{t}}\dot{\boldsymbol{q}}. \tag{36}$$

The complete Jacobian matrix of the mechanism can be obtained by simplifying (36):

$$\boldsymbol{J} = \boldsymbol{J}_{\mathrm{t}}^{-1}\boldsymbol{J}_{\mathrm{A}}\boldsymbol{T}_{\mathrm{a}}. \tag{37}$$

4 Performance analysis

4.1 Workspace analysis

In order to satisfy the needs of processing space for spherical crown surfaces, it is necessary to analyze the workspace performance of the hybrid mechanism. The workspace of the hybrid mechanism can be divided into a position workspace and a posture workspace. In this paper, the numerical search method is utilized to calculate the workspace.

4.1.1 Position workspace

The position workspace of the hybrid mechanism can be regarded as the overlapping area of the working space of the LAD, the parallel active branch and the passive constraint branch.

For constrained branch chains, the main factors affecting the workspace are: the moving distance of the P joint, and the rotation limit of the U joint and the R joint in the branch chain.

The rotation angle θ_{b} of the U joint and R joint in the passive branch should be satisfied as

$$-\theta_{\mathrm{bm}} \le \theta_{\mathrm{b}} \le \theta_{\mathrm{bm}} \tag{38}$$

where θ_{bm} represents the maximum rotation angle of the rotating joint in one direction.

The translation l_{b} of the passive P joint should be satisfied as

$$l_{\mathrm{b\,min}} \le l_{\mathrm{b}} \le l_{\mathrm{b\,max}} \tag{39}$$

where $l_{\mathrm{b\ min}}$ and $l_{\mathrm{b\ max}}$ represent the minimum and maximum translation of passive P joint, respectively.

For the driving part, the main factors affecting the workspace are the driving displacement of the LAD, the moving distance of the parallel actuated joint, and the length of the link.

The driving displacement r_{b} of the LAD should be satisfied as

$$r_{\mathrm{b\,min}} \le r_{\mathrm{b}} \le r_{\mathrm{b\,max}} \tag{40}$$

where $r_{\mathrm{b\ min}}$ and $r_{\mathrm{b\ max}}$ represent the minimum and maximum driving displacement of LAD, respectively.

The translation s_{i} (i=1, 2, $\cdots$, 5) of actuated P joint should be satisfied as

$$s_{\min} \le s_i \le s_{\max} \tag{41}$$

where $s_{\min}$ and $s_{\max}$ represent the minimum and maximum translation of actuated P joint, respectively.

The angle $\theta_{\mathrm{p}i}$ between the actuated link and the actuated direction of the P joint should be satisfied as

$$\theta_{\mathrm{p\,min}} \le \theta_{\mathrm{p}i} \le \theta_{\mathrm{p\,max}} \tag{42}$$

where $\theta_{\mathrm{p}i} = \arccos(\boldsymbol{s}_{i0}\boldsymbol{l}_{i0})$, $\theta_{\mathrm{p\ min}}$ and $\theta_{\mathrm{p\ max}}$ represent the minimum and maximum angle between the actuated link and the actuated direction of the P joint, respectively.

The angle $\theta_{\mathrm{d}i}$ between the actuated link and the moving platform should be satisfied as

$$\theta_{\mathrm{d\,min}} \le \theta_{\mathrm{d}i} \le \theta_{\mathrm{d\,max}} \tag{43}$$

where $\theta_{\mathrm{d}i} = \arccos\left(\dfrac{a_i\boldsymbol{l}_{i0}}{r_{\mathrm{a}}}\right)$, $\theta_{\mathrm{d\ min}}$ and $\theta_{\mathrm{d\ max}}$ represent the minimum and maximum angle between the actuated link and the moving platform, respectively.

An example of dimensional parameters and constraint range of the mechanism are given in Table 2.

Table 2 Parameters of mechanism

Parameter	Value	Parameter	Value
r_{c} (mm)	400	$s_{\min}$ (mm)	0
r_{a} (mm)	250	$s_{\max}$ (mm)	660
l (mm)	850	$\theta_{\mathrm{p\,min}}$ (°)	0
h_1 (mm)	90	$\theta_{\mathrm{p\,max}}$ (°)	90
g_2 (mm)	240	$\theta_{\mathrm{d\,min}}$ (°)	60
g_3 (mm)	70	$\theta_{\mathrm{d\,max}}$ (°)	160
l_1 (mm)	1 200	θ_{bm} (°)	60
$r_{\mathrm{b\,min}}$ (mm)	600	$l_{\mathrm{b\,min}}$ (mm)	350
$r_{\mathrm{b\,max}}$ (mm)	1 000	$l_{\mathrm{b\,max}}$ (mm)	700

For the 5PUS-2(UR)PU parallel mechanism part, the position workspace of the parallel mechanism can be obtained according to the constraints shown in Fig. 7. It can

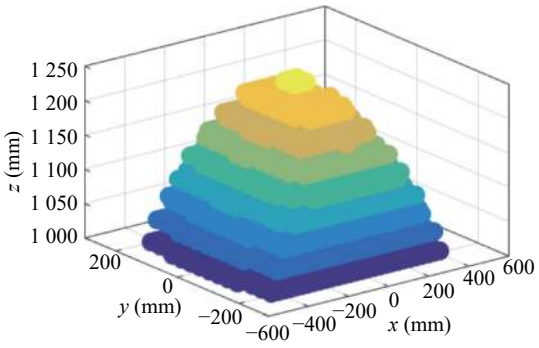

Fig. 7 Position workspace of parallel mechanism

be seen from Fig. 7 that the vertical displacement of only the parallel mechanism is about 230 mm.

When the posture angles α and β are both zero, the position workspace of the hybrid mechanism is shown in Fig. 8. It can be seen from Fig. 8 that the workspace of the hybrid mechanism is 1 200 mm at the lowest position in the vertical z direction and 3 500 mm at the highest position.

Comparing the position workspace of the parallel mechanism and the hybrid mechanism, it can be seen from Figs. 7 and 8 that the vertical displacement of the hybrid mechanism is about 10 times that of the parallel mechanism. Therefore, the workspace of the mechanism is increased by the way of mixed connection. At the same time, the stroke-to-size ratio of the hybrid mechanism is as high as 292%, and the mechanism has a large workspace. This parameter can be used as a reference for the design of the actual processing mechanism.

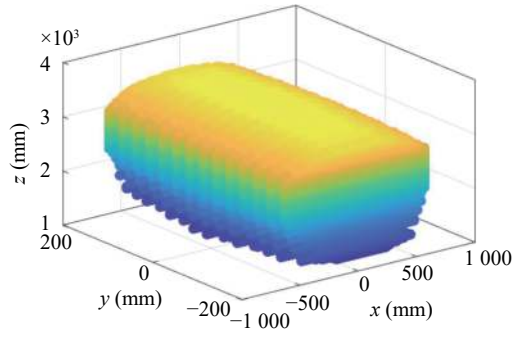

(a) Position workspace

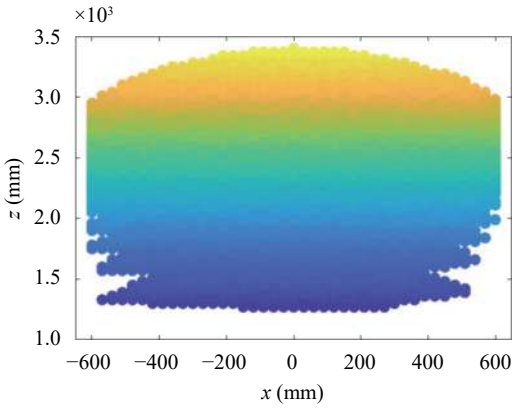

(b) Main view

Fig. 8 Position workspace of hybrid mechanism and its main view

4.1.2 Posture workspace

The analysis method is the same as the position workspace. According to the constraint conditions and given the coordinates ${}^{\mathrm{B}}A = (x, y, z)$ of the center point A, the posture workspace when ${}^{\mathrm{B}}A = (0, 0, 900)$, ${}^{\mathrm{B}}A = (0, 0, 980)$ are shown in Figs. 9 (a) and (b), respectively.

It can be seen from Fig. 9 that the maximum rotation angle range of the hybrid mechanism is ±35°. The mechanism has good posture ability.

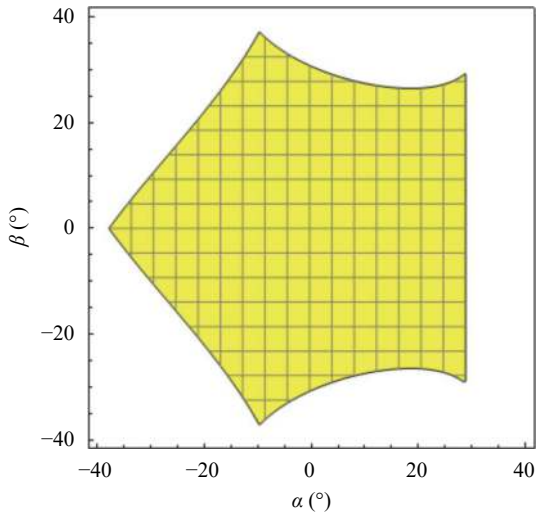

(a) Posture workspace when z = 900 mm

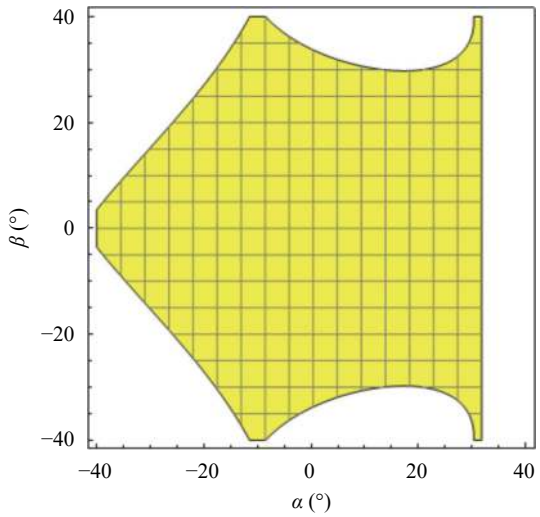

(b) Posture workspace when z = 980 mm

Fig. 9 Posture workspace of hybrid mechanism

4.2 Dexterity analysis

The Jacobian condition number can be used as a dexterity index for a purely translational or purely rotating

parallel mechanism. However, for a 5-DOF parallel robot mechanism that has both rotation and translation, its conclusion cannot be guaranteed. Therefore, local condition indicators are used for analysis.

For the velocity Jacobian matrix, write it as an inverse Jacobian matrix:

$$\boldsymbol{J}^{-1}\dot{\boldsymbol{q}} = \begin{bmatrix} \dot{\alpha} \\ \dot{\beta} \\ v \end{bmatrix}. \tag{44}$$

Because the dimensions are not uniform, (44) can be rewritten as

$$\begin{bmatrix} \dot{\alpha} \\ \dot{\beta} \end{bmatrix} = \boldsymbol{J}_1\boldsymbol{q} \tag{45}$$

$$\boldsymbol{V} = \boldsymbol{J}_2\boldsymbol{q} \tag{46}$$

where $\boldsymbol{J}_1$ is a 2×5 matrix composed of the first two lines of $\boldsymbol{J}^{-1}$, $\boldsymbol{J}_2$ is a 3×5 matrix composed of the last three lines of $\boldsymbol{J}^{-1}$.

Then, the condition numbers of the matrices $\boldsymbol{J}_1$ and $\boldsymbol{J}_2$ can be obtained as

$$\begin{cases} \kappa_{J_\omega} = \sigma_{\omega 1}/\sigma_{\omega 2} \\ \kappa_{J_v} = \sigma_{v1}/\sigma_{v2} \end{cases} \tag{47}$$

where $\sigma_{\omega 1}$ and $\sigma_{\omega 2}$ are the maximum singular value and minimum singular value of matrix $\boldsymbol{J}_1$ respectively, σ_{v1} and σ_{v2} are the maximum singular value and minimum singular value of matrix $\boldsymbol{J}_2$ respectively. κ_{J_ω} and κ_{J_v} are angular velocity and linear velocity isotropic indexes, respectively, which are used to evaluate the dexterity of the angular velocity and linear velocity of the robot, respectively.

When $x = 0$, $y = 0$, $z = 950$ mm, the angular velocity and linear velocity condition number distributions with the rotation angles α and β based on the parameters in Table 2 are shown in Figs. 10(a) and (b), respectively. The maximum values of κ_{J_ω} and κ_{J_v} are 2.4 and 20, respectively.

When $\alpha = 0$, $\beta = 0$, $z = 950$ mm, the angular velocity and linear velocity condition number distributions with displacement x, y and z based on the parameters in Table 2 are shown in Figs. 11(a) and (b), respectively. The maximum values of κ_{J_ω} and κ_{J_v} are 1.45 and 8, respectively. It can be seen from Figs. 10 and 11 that the value of the condition number is small, the change is stable, and there are no sudden changes in the entire workspace. The mechanism has good dexterity.

4.3 Stiffness analysis

To analyze the stiffness change of the mechanism during the movement, the most commonly used method is to

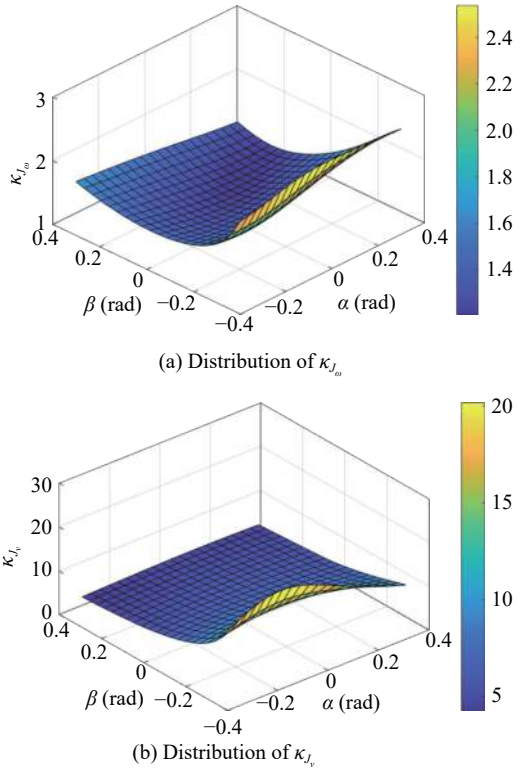

(a) Distribution of κ_{J_ω}

(b) Distribution of κ_{J_v}

Fig. 10 Distribution of condition numbers when $x = 0$, $y = 0$, $z = 950$ mm

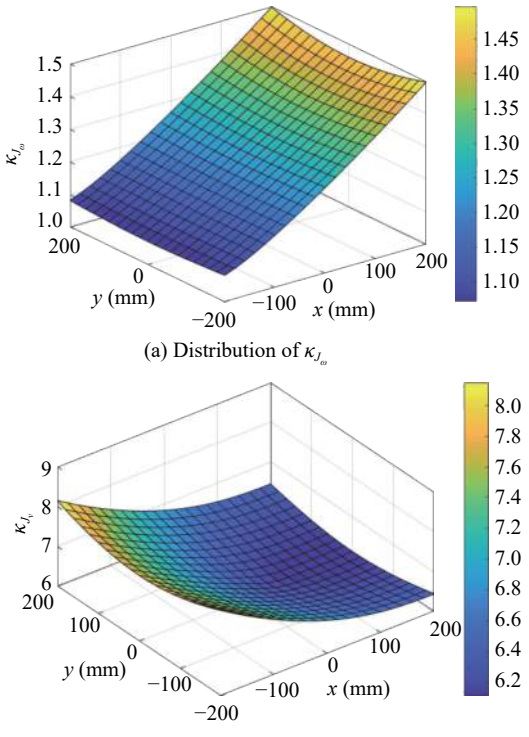

(a) Distribution of κ_{J_ω}

(b) Distribution of κ_{J_v}

Fig. 11 Distribution of condition number when $\alpha = 0$, $\beta = 0$, $z = 950$ mm

solve the stiffness matrix of the mechanism[28]. The stiffness matrix of the mechanism can be expressed as

$$\boldsymbol{K} = \boldsymbol{J}^{\mathrm{T}}\boldsymbol{\chi}\boldsymbol{J} \tag{48}$$

where $\boldsymbol{K}$ is the stiffness matrix, $\boldsymbol{J}$ is the Jacobian matrix of the mechanism, $\boldsymbol{\chi} = \mathrm{diag}(k_1, k_2, \cdots, k_i)$, $k_i (i{=}1, 2, \cdots, 5)$ is the equivalent spring coefficient of each joint. Here, k_i is set to 1 000 N/mm[29].

The relationship between the equivalent force screw F of the moving platform and its small deformation amount ΔX is

$$\boldsymbol{F} = \boldsymbol{K}\Delta\boldsymbol{X}. \tag{49}$$

The minimum eigenvalue of the stiffness matrix $\boldsymbol{K}$ is selected as an index to evaluate the stiffness performance. When the position of the moving platform is fixed, i.e., $x = 0$, $y = 0$, and $z = 950$ mm, the distribution of the stiffness with the rotation angles α and β is shown in Fig. 12. It can be seen from Fig. 12 that when the absolute value of α is small, the overall stiffness value is small.

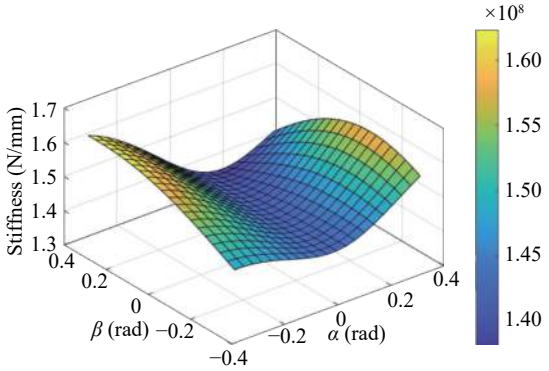

Fig. 12 Distribution of stiffness when $x{=}0$, $y = 0$, $z = 950$ mm

When the posture angles of the moving platform are fixed, i.e., $\alpha = 0$, $\beta = 0$, the distribution of stiffness with displacement x, y and z is shown in Figs. 13. It can be seen from Fig. 13 that the stiffness of the moving platform increases as the absolute values of x, y and z increase. In general, the value of the stiffness at different locations in the workspace is mostly above 100 kN/m. And the stiffness performance of the mechanism is good in the entire workspace.

5 Simulation analysis

In this section, in order to verify the correctness of the mechanism design and kinematic model, the theoretical calculation and simulation analysis of the hybrid mechanism with arc curve as the processing trajectory are carried out by using Matlab and Adams software. The theoretical and simulation curves of the driving parameters of

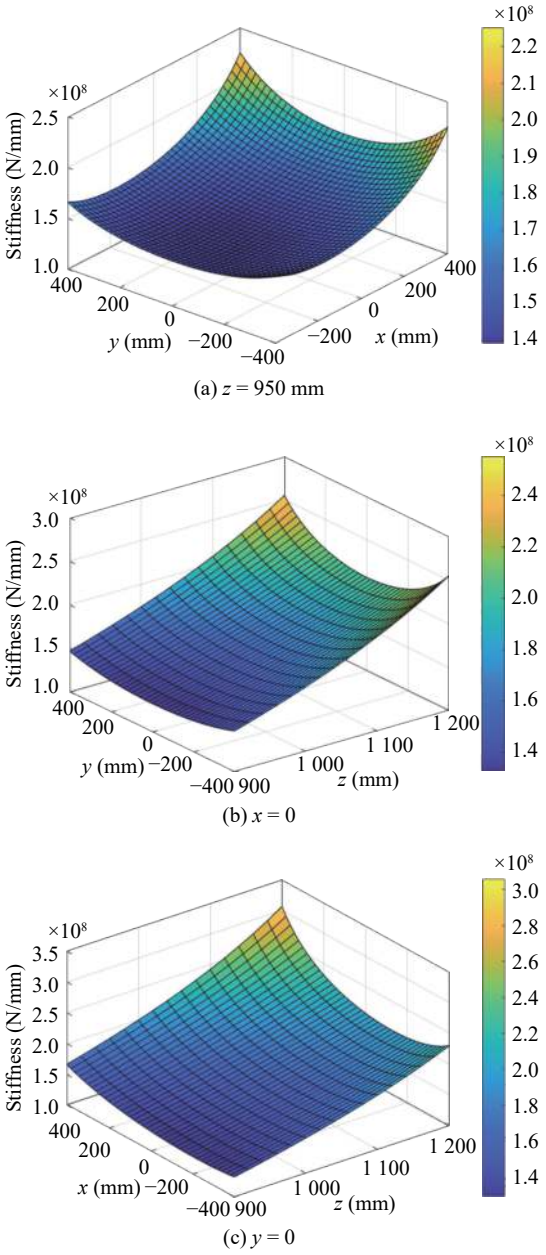

Fig. 13 Distribution of stiffness when $\alpha = 0$, $\beta = 0$

the P joint are compared and analyzed.

The moving platform center is used as the position of the machining tool, and the arc curve is used as the machining trajectory to complete the kinematic simulation. The motion trajectory of the processing tool is shown in Figs. 14 (a) and (b). The tool moves from the Q point to a circle at a constant speed along the arc trajectory and returns to the Q point. Assume that the radius of the arc trajectory is 20 mm, the time t of the simulation movement is 20 s, and the initial position of the moving platform is parallel to the fixed platform. Because it is a plane motion, the tool rotation angles α and β are 0, and the z-axis direction is a constant value. Then the driving equation can be obtained as

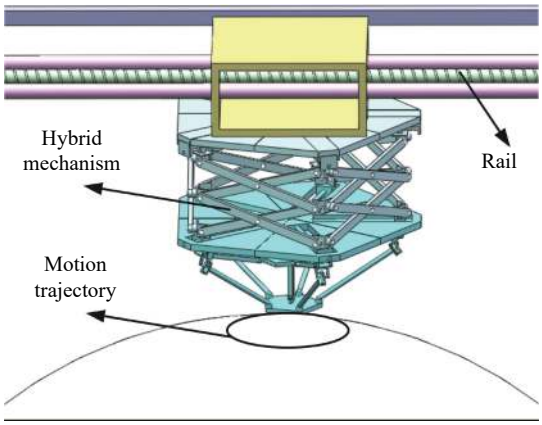

(a) Motion trajectory in the overall mechanism

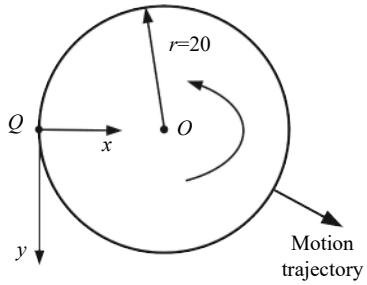

(b) Parameters of the motion trajectory

Fig. 14 Motion trajectory of simulation

$$\begin{cases} x = 20 + r\cos(0.1t \times \pi - \pi) \\ y = r\sin(0.1t \times \pi - \pi). \end{cases} \tag{50}$$

Substituting (50) into the inverse kinematics (14), according to the motion trajectory of the moving platform, the corresponding theoretical displacement of each actuated P joint can be calculated. And the velocity and acceleration of each actuated P joint can be obtained by the first and second derivative of time. A virtual prototype simulation model of the mechanism is established in Adams, and (50) is used as the driving equation of the moving platform center in the simulation model. Then, the simulation curve of the translation, velocity, and acceleration of the actuated P joint can be obtained. The comparison between the theoretical calculation curve and the simulation curve of the translation, velocity, and acceleration of each actuated P joint is shown in Fig. 15. The solid line in Fig. 15 is the theoretical curve of the actuated joint calculated by Matlab software. The dashed line marked with the character "o" is a simulation curve of motion parameters obtained from Adams software.

It can be seen from Fig. 15 that the theoretical calculation curve of the translation, velocity and acceleration of the actuated P joint coincides with the simulation curve. And the simulation results verify the correctness of the theoretical calculation. At the same time, the curve of each actuated joint is smooth and continuous, with no sudden changes such as sharp points, which proves that the mechanism can achieve the motion ability of a given trajectory.

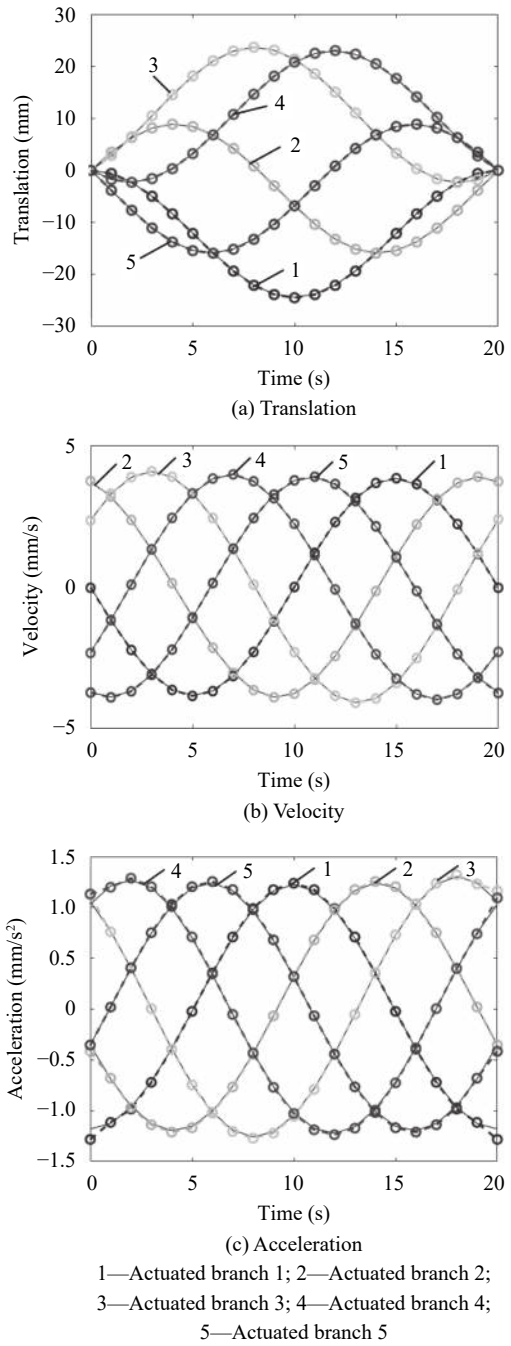

(a) Translation

(b) Velocity

(c) Acceleration

Fig. 15 Theory and simulation kinematics curve of actuated joint

6 Conclusions

1) A novel 5PUS-(2UR)PU hybrid robot mechanism is designed for the processing of spherical crown surface on oversized cylindrical boxes. The workspace of the mechanism is increased by connecting the LAD in series with the parallel mechanism. By using the parallel mechanism as a local processing head, the overall dexterity of the mechanism is improved.

2) The degrees of freedom of the parallel mechanism are obtained by using the screw theory, and the result satisfied the processing requirement of 5 degrees of freedom. Constraints affecting workspace are established, and the workspace of the mechanism is solved. The dexterity and stiffness analyses are obtained on the basis of the Jacobian matrix. The stroke-to-size ratio of the designed hybrid mechanism is as high as 292%, and it has a large workspace. In the effective workspace, the dexterity index of the mechanism is less than 5, and the mechanism has high dexterity. The value of the stiffness at different locations is mostly above 100 kN/m. And the stiffness performance of the mechanism is good in the entire workspace.

3) The theoretical calculation and simulation analysis of the hybrid mechanism with arc curve as the processing trajectory are carried out by using Matlab and Adams software. The theoretical calculation curve of the translation, velocity and acceleration of the actuated P joint coincides with the simulation curve, and the simulation results verify the correctness of the theoretical calculation. At the same time, the curve of each actuated joint is smooth and continuous, with no sudden changes such as sharp points, which proves that the mechanism can achieve the motion ability of a given trajectory.

Acknowledgements

This work was supported by Fundamental Research Funds for the Central Universities (No. 2018JBZ007).

References

[1] C. S. G. Lee, M. Ziegler. Geometric approach in solving inverse kinematics of PUMA robots. *IEEE Transactions on Aerospace and Electronic Systems*, vol. AES-20, no. 6, pp. 695–706, 1984. DOI: 10.1109/TAES.1984.310452.

[2] A. Omodei, G. Legnani, R. Adamini. Three methodologies for the calibration of industrial manipulators: Experimental results on a SCARA robot. *Journal of Robotic Systems*, vol. 17, no. 6, pp. 291–307, 2000.

[3] A. Nubiola, I. A. Bonev. Absolute calibration of an ABB IRB 1600 robot using a laser tracker. *Robotics and Computer-Integrated Manufacturing*, vol. 29, no. 1, pp. 236–245, 2013. DOI: 10.1016/j.rcim.2012.06.004.

[4] A. Pashkevich, D. Chablat, P. Wenger. Stiffness analysis of overconstrained parallel manipulators. *Mechanism and Machine Theory*, vol. 44, no. 5, pp. 966–982, 2009. DOI: 10.1016/j.mechmachtheory.2008.05.017.

[5] H. Q. Zhang, H. R. Fang, B. S. Jiang. Motion-force transmissibility characteristic analysis of a redundantly actuated and overconstrained parallel machine. *International Journal of Automation and Computing*, vol. 16, no. 2, pp. 150–162, 2019. DOI: 10.1007/s11633-018-1156-5.

[6] B. S. Jiang, H. R. Fang, H. Q. Zhang. Type synthesis and kinematics performance analysis of a class of 3T2R parallel mechanisms with large output rotational angles. *International Journal of Automation and Computing*, vol. 16, no. 6, pp. 775–785, 2019. DOI: 10.1007/s11633-019-1192-9.

[7] M. Mazare, M. Taghizadeh, M. R. Najafi. Kinematic analysis and design of a 3-DOF translational parallel robot. *International Journal of Automation and Computing*, vol. 14, no. 4, pp. 432–441, 2017. DOI: 10.1007/s11633-017-1066-y.

[8] Z. Gao, D. Zhang. Performance analysis, mapping, and multiobjective optimization of a hybrid robotic machine tool. *IEEE Transactions on Industrial Electronics*, vol. 62, no. 1, pp. 423–433, 2015. DOI: 10.1109/TIE.2014.2327008.

[9] F. Gao, B. B. Peng, H. Zhao, W. M. Li. A novel 5-DOF fully parallel kinematic machine tool. *The International Journal of Advanced Manufacturing Technology*, vol. 31, no. 1-2, pp. 201–207, 2006. DOI: 10.1007/s00170-005-0171-1.

[10] S. Kucuk. Dexterous workspace optimization for a new hybrid parallel robot manipulator. *Journal of Mechanisms and Robotics*, vol. 10, no. 6, Article number 064503, 2018. DOI: 10.1115/1.4041334.

[11] T. K. Tanev. Kinematics of a hybrid (parallel-serial) robot manipulator. *Mechanism and Machine Theory*, vol. 35, no. 9, pp. 1183–1196, 2000. DOI: 10.1016/S0094-114X(99)00073-7.

[12] F. G. Xie, X. J. Liu, H. Zhang, J. S. Wang. Design and experimental study of the SPKM165, a five-axis serial-parallel kinematic milling machine. *Science China Technological Sciences*, vol. 54, no. 5, pp. 1193–1205, 2011. DOI: 10.1007/s11431-011-4314-3.

[13] F. Q. Zhao, S. Guo, Z. C. Xu, D. Li. Design and analysis of high performance machine tool based on redundant parallel mechanism. *Journal of Central South University* (*Science and Technology*), vol. 50, no. 1, pp. 67–74, 2019. DOI: 10.11817/j.issn.1672-7207.2019.01.010. (in Chinese)

[14] B. Siciliano. The Tricept robot: Inverse kinematics, manipulability analysis and closed-loop direct kinematics algorithm. *Robotica*, vol. 17, no. 4, pp. 437–445, 1999. DOI: 10.1017/S0263574799001678.

[15] Z. M. Bi, Y. Jin. Kinematic modeling of Exechon parallel kinematic machine. *Robotics and Computer-Integrated Manufacturing*, vol. 27, no. 1, pp. 186–193, 2011. DOI: 10.1016/j.rcim.2010.07.006.

[16] Y. Q. Zhao, Y. Jin, J. Zhang. Kinetostatic modeling and analysis of an exechon parallel kinematic machine (PKM) module. *Chinese Journal of Mechanical Engineering*, vol. 29, no. 1, pp. 33–44, 2016. DOI: 10.3901/CJME.2015.1012.120.

[17] B. B. Lian, T. Sun, Y. M. Song, Y. Jin, M. Price. Stiffness analysis and experiment of a novel 5-DOF parallel kinematic machine considering gravitational effects. *International Journal of Machine Tools and Manufacture*, vol. 95, pp. 82–96, 2015. DOI: 10.1016/j.ijmachtools.2015.04.012.

[18] T. Huang, M. Li, X. M. Zhao, J. P. Mei, D. G. Chetwynd, S. J. Hu. Conceptual design and dimensional synthesis for a 3-DOF module of the TriVariant-a novel 5-DOF reconfigurable hybrid robot. *IEEE Transactions on Robotics*, vol. 21, no. 3, pp. 449–456, 2005. DOI: 10.1109/TRO.2004.840908.

[19] H. T. Liu, T. Huang, J. P. Mei, X. M. Zhao, D. G. Chetwynd, M. Li, S. J. Hu. Kinematic design of a 5-DOF hybrid robot with large workspace/limb-stroke ratio. *Journal of Mechanical Engineering*, vol. 129, no. 5, pp. 530–537, 2007. DOI: 10.1115/1.2712220.

[20] C. L. Dong, H. T. Liu, W. Yue, T. Huang. Stiffness modeling and analysis of a novel 5-DOF hybrid robot. *Mechan-*

ism and Machine Theory, vol. 125, pp. 80–93, 2018. DOI: 10.1016/j.mechmachtheory.2017.12.009.

[21] Y. M. Song, B. B. Lian, T. Sun, G. Dong, Y. Qi, H. Gao. A novel five-degree-of-freedom parallel manipulator and its kinematic optimization. *Journal of Mechanisms and Robotics*, vol. 6, no. 4, Article number 041008, 2014. DOI: 10.1115/1.4027742.

[22] H. Yang, H. R. Fang, Y. F. Fang, H. B. Qu. Kinematics performance and dynamics analysis of a novel parallel perfusion manipulator with passive link. *Mathematical Problems in Engineering*, vol. 2018, Article number 6768947, 2018. DOI: 10.1155/2018/6768947.

[23] H. Yang, H. R. Fang, D. Li, Y. F. Fang. Kinematics analysis and multi-objective optimization of a novel parallel perfusion robot. *Journal of Beijing University of Aeronautics and Astronautics*, vol. 44, no. 3, pp. 568–575, 2018. DOI: 10.13700/j.bh.1001-5965.2017.0157. (in Chinese)

[24] M. Toz, S. Kucuk. Dimensional optimization of 6-DOF 3-CCC type asymmetric parallel manipulator. *Advanced Robotics*, vol. 28, no. 9, pp. 625–637, 2014. DOI: 10.1080/01691864.2014.884935.

[25] F. G. Xie, X. J. Liu, Z. You, J. S. Wang. Type synthesis of 2T1R-type parallel kinematic mechanisms and the application in manufacturing. *Robotics and Computer-Integrated Manufacturing*, vol. 30, no. 1, pp. 1–10, 2014. DOI: 10.1016/j.rcim.2013.07.002.

[26] Y. Kakinuma, K. Igarashi, S. Katsura, T. Aoyama. Development of 5-axis polishing machine capable of simultaneous trajectory, posture, and force control. *CIRP Annals*, vol. 62, no. 1, pp. 379–382, 2013. DOI: 10.1016/j.cirp.2013.03.135.

[27] D. C. Zhu, Z. M. Yan, X. F. Cui, P. Li. Kinematics analysis and simulation of 3-RPS-type parallel robot based on screw theory. *Mechanical Science and Technology for Aerospace Engineering*, vol. 32, no. 1, pp. 28–31, 2013. DOI: 10.13433/j.cnki.1003-8728.2013.01.010. (in Chinese)

[28] G. Coppola, D. Zhang, K. F. Liu. A 6-DOF reconfigurable hybrid parallel manipulator. *Robotics and Computer-Integrated Manufacturing*, vol. 30, no. 2, pp. 99–106, 2014. DOI: 10.1016/j.rcim.2013.09.011.

[29] X. J. Liu, Z. L. Jin, F. Gao. Optimum design of 3-DOF spherical parallel manipulators with respect to the conditioning and stiffness indices. *Mechanism and Machine Theory*, vol. 35, no. 9, pp. 1257–1267, 2000. DOI: 10.1016/S0094-114X(99)00072-5.

Hai-Rong Fang received the B. Eng. degree in mechanical engineering from Nanjing University of Science and Technology, China in 1990, the M. Eng. degree in mechanical engineering from Sichuan University, China in 1996, and the Ph. D. degree in mechanical engineering from Beijing Jiaotong University, China in 2005. She worked as an associate professor in Department of Engineering Mechanics, Beijing Jiaotong University, China from 2003 to 2011. She is a professor in School of Mechanical Engineering from 2011 and director of Robotics Research Center.

Her research interests include parallel mechanisms, digital control, robotics and automation, and machine tool equipment.

E-mail: hrfang@bjtu.edu.cn (Corresponding author)

ORCID iD: 0000-0001-7938-4737

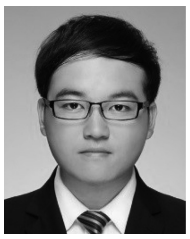

Tong Zhu received the B. Eng. degree in mechanical engineering from Beijing Jiaotong University, China in 2017. Currently, he is a master student at School of Mechanical, Electronic and Control Engineering, Beijing Jiaotong University, China.

His research interests include robotics in computer integrated manufacturing and parallel kinematics machine tool.

E-mail: 17121313@bjtu.edu.cn

ORCID iD: 0000-0001-9845-004X

Hai-Qiang Zhang received the B. Eng. degree in mechanical design and theories from Yantai University, China in 2012, the M. Eng. degree in mechanical engineering from Hebei University of Engineering, China in 2015. He is a Ph. D. degree candidate at Beijing Jiaotong University, China.

His research interests include robotics in computer integrated manufacturing, parallel kinematics machine tool, redundant actuation robots, over-constrained parallel manipulators, and multi-objective optimization design.

E-mail: 16116358@bjtu.edu.cn

ORCID iD: 0000-0003-4421-5671

Hui Yang received the B. Eng. degree in mechanical engineering from Beijing Jiaotong University, China in 2014. She is currently a Ph. D. degree candidate at School of Mechanical, Electronic and Control Engineering, Beijing Jiaotong University, China.

Her research interests include robotics in computer integrated manufacturing and parallel kinematics machine tool.

E-mail: 15116342@bjtu.edu.cn

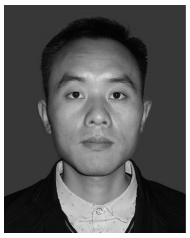

Bing-Shan Jiang received the B. Eng. degree in mechanical electronic engineering from Liaoning Technical University, China in 2015, and the M. Eng. degree in mechanical engineering from Liaoning Technical University, China in 2017. He is currently a Ph. D. degree candidate at School of Mechanical, Electronic and Control Engineering, Beijing Jiaotong University, China.

His research interests include synthesis, kinematics, dynamics and control of parallel robots.

E-mail: 17116381@bjtu.edu.cn

ORCID iD: 0000-0002-9471-8309